Thin Solid Films 520 (2011) 1313–1317

Contents lists available at ScienceDirect

Thin Solid Films

journal homepage: www.elsevier.com/locate/tsf

Optical modelling of fluorine doped ZnO

R.E. Treharne *, K. Durose

Department of Physics, Durham University, Science Site, South Road, Durham DH1 3LE, United Kingdom

ARTICLE INFO

Available online 30 April 2011

Keywords:
Fluorine doped ZnO
RF magnetron sputtering
Dielectric modelling
CdTe/CdS solar cells

ABSTRACT

A model for the complex dielectric function appropriate for use with fluorine doped ZnO transparent conductors has been developed. The model uses three components; a Drude term, a Lorentz oscillator, and a term accounting for inter-band transitions. It was used to generate the complex dielectric permittivity for ZnO:F, which in turn was used to fit experimentally determined optical transmission data for sputtered films. Use of this methodology to provide data for modelling the optical transmission through the window layer stacks of solar cell devices is commented upon. The experimentally determined Burstein–Moss shifts and carrier concentrations for a series of films were used to calculate a value of $m_e = 0.33 \pm 0.8\ m_0$ according to the model's assumptions.

1. Introduction

Doped ZnO films offer a promising alternative to indium tin oxide (ITO) as a transparent conducting front contact layer in CdTe/CdS solar cells. The substitutional doping of ZnO films with group III metals such as Al, B and Ga has been widely reported [1–3], however out-diffusion of the electrically active metal dopants during subsequent cell fabrication procedures can lead to detrimental effects on device performance. It has been shown, using reactive RF sputtering, that ZnO films can instead be doped with fluorine and maintain comparable electrical and optical properties to those of the group III doped films [4–6]. Such films should be better suited for maintaining stability in CdTe/CdS solar cells where the diffusion of F out of the layer during subsequent high temperature fabrication of CdS and CdTe layers is unlikely to cause a significant degradation in device performance.

In this work, a model of the complex dielectric permittivity $\varepsilon(\omega)$ for fluorine doped ZnO films is presented in the range of frequencies relevant to CdTe/CdS solar cell design (i.e. UV—near IR). The model draws upon classical Drude and Lorentz theories for the optical behaviour of metals and insulators respectively, as well as an inter-band transition model necessary for describing behaviour in the region of direct and indirect band gaps. The model is tested through its use in fitting experimental transmission data from sputtered ZnO:F films on glass substrates. The aim is to develop a model for accurate extraction of $n(\omega)$, $\kappa(\omega)$, band gap, Burstein–Moss shift, carrier concentration and mobility, from a single transmission measurement. Such a tool would permit the rapid characterisation of combinatorial sample libraries in which a deliberate doping gradient is incorporated over the surface of a single film.

2. Experimental details

Film deposition was achieved using an AJA Orion Phase II-J sputtering system with an unbalanced magnetron configuration. A series of films were reactively sputtered from a 75 mm diameter ceramic ZnO target (purity 99.999%, PI-KEM Ltd.) in 5 mTorr (6.7×10^{-3} mbar) of Ar with a constant 5% partial pressure of H_2 and a CHF_3 partial pressure varied in the range 1–7%. An undoped, highly stochiometric ZnO film was prepared as a standard by sputtering in Ar with a 5% partial pressure of O_2. A constant sputter power and substrate temperature of 100 W and 350 °C respectively was maintained throughout. $50 \times 50 \times 3\ mm^3$ substrates of low-Fe soda lime glass (Optiwhite™, Pilkington) were cleaned prior to deposition by scrubbing with a nylon brush and de-ionised water, followed by an isopropanol alcohol rinse and N_2 blow dry. The substrate surfaces were then plasma etched in-situ for 10 min prior to deposition.

Transmission measurements were performed in the range 250–1500 nm using a Shimadzu Solid-Spec UV–VIS-IR 3700 spectrophotometer. Values for the effective direct band gap E_d' of the films were extrapolated from plots of $(\alpha\hbar\omega)^2$ vs $\hbar\omega$ where α is the linear absorption coefficient determined from transmission measurements and taking into account the effect of the substrate. The experimental Burstein–Moss shifts, Δ_{BM}^{exp}, for each sample were then calculated according to $\Delta_{BM}^{exp} = E_d' - E_d$, where E_d is the direct band gap of an undoped, stochiometric film. Initial estimates of film thickness, d_S were calculated analytically from the fringe profile of the transmission spectra, at frequencies below the band gap, according to Swanepoel's envelope method [7,8]. The free carrier density n_e^H and mobility μ_e^H

* Corresponding author.
E-mail address: R.Treharne@liverpool.ac.uk (R.E. Treharne).

0040-6090/$ – see front matter © 2011 Elsevier B.V. All rights reserved.
doi:10.1016/j.tsf.2011.04.155

were determined from Hall measurents made in the van der Pauw configuration using custom built equipment.

3. A description of the optical model

Over the range of interest for CdTe solar cell optical absorption (250–1500 nm), the dielectric permittivity of the material was modelled using three separate components. The first two correspond to the classical theories of Lorentz and Drude and account for the behaviour of bound and free electrons respectively. The third draws upon a quantum mechanical description of the transitions of excited electrons from the material's valence band to its conduction band in order to predict the optical behaviour in the region of a band gap. Thus, the complete form of the complex dielectric function may be calculated from the sum of these three components according to

$$\varepsilon(\omega) = \varepsilon_1 + i\varepsilon_2 = \varepsilon_{\text{Lorentz}} + \varepsilon_{\text{Drude}} + \varepsilon_{IB} \tag{1}$$

where ε_1 and ε_2 are the real and imaginary components respectively, and the subscript IB denotes 'inter-band' transitions. Similar methodologies have been reported for the modelling of Al and In doped ZnO [9–11] as well as Sn doped In_2O_3 [12].

A useful quantity for the subsequent generation of theoretical transmission spectra is the complex refractive index $\tilde{n}$ which can be calculated from $\varepsilon(\omega)$ as

$$\tilde{n} = n + i\kappa = \sqrt{\varepsilon_1 + i\varepsilon_2} \tag{2}$$

where n is the refractive index and κ is the extinction coefficient. Using this, transmission spectra were generated using commercial software [13] and the parameters within each of the model components were determined by fitting the theoretical spectra to those determined experimentally via a downhill simplex method. The quality of the fits were determined by the mean squared error, MSE, calculated by considering the resultant differences in experimental and theoretical spectra. Values of MSE <10 were considered a good fit, while values <1 were deemed excellent.

3.1. Classical models

A single Lorentz oscillator was incorporated into the model according to [14]

$$\varepsilon_{\text{Lorentz}} = 1 + \frac{A_1}{\omega_0^2 - \omega^2 - i\omega\gamma_1} \tag{3}$$

where A_1 is the oscillator amplitude, ω_0 is the resonant frequency and γ_1 is a damping term. The value of ω_0 is likely to correspond to a frequency well outside the model's range of interest (i.e. ≪250 nm), and so the accurate determination of the oscillator's parameters is not crucial. It is sufficient that the parameter values give rise to a slowly varying (almost constant) dielectric background within the region of interest.

The functional form of the Drude component is given by [15,16]

$$\varepsilon_{\text{Drude}} = -\frac{\sigma_0}{\varepsilon_0}\left(\frac{\tau}{1+\omega^2\tau^2}\right) + \frac{i\sigma_0}{\omega\varepsilon_0}\left(\frac{1}{1+\omega^2\tau^2}\right) \tag{4}$$

where τ is the scattering time of the free carriers and σ_0 is the d.c. electrical conductivity defined as

$$\sigma_0 = \frac{n_e e^2 \tau}{m_e} = n_e e \mu_e \tag{5}$$

where μ_e defines mobility of the free electrons within the material.

3.2. Inter-band transition model

The component of the dielectric permittivty ε_{IB} can be further reduced to two components according to

$$\varepsilon_{IB} = \varepsilon_d + \varepsilon_i \tag{6}$$

where the subscripts d and i denote direct and indirect transitions respectivtely. A simple parabolic band model [17] was used to describe the relative shapes of the valence and conduction bands in the vicinity of the material's direct band gap (Fig. 1). By assigning the bottom of the conduction band as being at $E=0$ when $k=0$, the conduction and valence band energies, E_c and E_v, may be expressed as

$$E_c = \frac{\hbar^2 k^2}{2m_e} \tag{7}$$

$$E_v = -E_d - \frac{\hbar^2 k^2}{2m_h} \tag{8}$$

where m_e and m_h are the effective masses of electrons and holes within the conduction and valence bands respectively. The material's direct band gap is denoted by E_d. The photon energies that are permitted to take part in inter-band transition processes (i.e. $E>E_d$) may thus be written in the following terms

$$\hbar\omega = E_c - E_v = E_d + \frac{\hbar^2 k^2}{2}\left(\frac{1}{m_e} + \frac{1}{m_h}\right). \tag{9}$$

The functional form of the imaginary component of ε_d may initially be expressed as [18]

$$\varepsilon_{2_d} = \frac{P_d}{\omega^2}\left(\hbar\omega - E_g\right)^{1/2} \tag{10}$$

where P_d is the probability amplitude of the transition of an electron from the valence to the conduction band. This expression alone would be enough to describe behaviour in an undoped film. However, in the case of heavily doped material, there are enough donors present for states in the conduction band to be partially filled. Hence, the

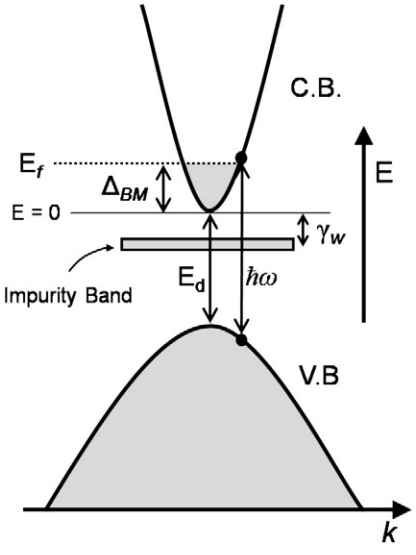

Fig. 1. A schematic of the parabolic band model which is used to describe the optical behaviour due to inter-band transitions in ZnO:F films. In a heavily doped film ($n_e > 10^{19}$ cm^{-3}), the conduction band is filled to the Fermi energy $E_f = \Delta_{BM}$. An impurity band located within the energy gap gives rise to an exponential absorption tail ('Urbach' tail) at energies below E_d. The relative shape of the valence and conduction bands is described by the ratio m_e/m_h.

probability that states in the conduction band are already occupied is given by the Fermi–Dirac function

$$F_e = \left(1 + \exp\frac{E_c - \Delta_{BM}}{kT}\right)^{-1} \tag{11}$$

$$= \left(1 + \exp\frac{\frac{1}{1 + m_e/m_h}(\hbar\omega - E_d) - \Delta_{BM}}{kT}\right)^{-1} \tag{12}$$

where the parameter Δ_{BM} is defined as the Burstein–Moss shift [19,20] and, as shown in Fig. 1, for a degenerate semiconductor, is equivalent to the energy difference between the Fermi level and the conduction band minimum i.e.

$$E_f = \Delta_{BM} = \frac{\hbar^2}{2m_e}(3\pi n_e)^{2/3}. \tag{13}$$

Eq. (9) may now be re-written as

$$\varepsilon_{2_d} = \frac{P_d}{\omega^2}(\hbar\omega - E_d)^{1/2}[1 - F_e]. \tag{14}$$

It is implicit in Eq. (13) that the effect on the Fermi level position is solely due to the BM shift, an assumption that is discussed in Section 4.

Further to this, it was necessary to model the effects that localised impurities, namely oxygen vacancies and interstitial fluorine atoms, have on the shape of ε_{2_d}. Fig. 1 shows an impurity band located in the forbidden gap. It is assumed that the states in this band may overlap with those in the conduction band. The effects of this band can be expressed by augmenting Eq. (12) with an exponential tail at energies below the band gap [21].

$$\varepsilon_{2_d} = \begin{cases} \frac{P_d}{\omega^2}(\hbar\omega - E_d)^{1/2}[1 - F_e] & \text{if } \hbar\omega > E_d + \Delta_{BM} \\ \exp\frac{\frac{1}{1 + m_e/m_h}(\hbar\omega - E_d) - \Delta_{BM}}{\gamma_w} & \text{if } \hbar\omega < E_d + \Delta_{BM} \end{cases} \tag{15}$$

where γ_w describes the extent of the exponential tail into the energy gap.

During an indirect transition, an electron in the valence band undergoes an interaction with both a photon, $\hbar\omega$, and a phonon, E_p, and is consequently promoted to the valence band. The incident photon energy that permits an indirect transition may be expressed as

$$\hbar\omega = E_c(k') - E_v(k) \pm E_p \tag{16}$$

where k and k' are the electron's momentum before and after the transition respectively. Note that because the phonon possesses a finite momentum it is not necessary that $k' = k$ as with a direct transition. The $\pm$ sign in this equation indicates that phonons can be absorbed or emitted during the process. From second order perturbation theory [18,22] the component of the dielectric permittivity due to indirect transitions may be derived as

$$\varepsilon_{2_i} = \frac{P_i}{\omega^2}\left\{\frac{\left(\hbar + E_p - E_i\right)}{\exp\left(E_p/kT\right)} + \frac{\left(\hbar\omega - E_p - E_i\right)}{1 - \exp\left(-E_p/kT\right)}\right\} \tag{17}$$

where E_i is the indirect band gap and P_i is the probability amplitude of an indirect transition of an electron from the valence band to the conduction band.

Knowing the functional form of $\varepsilon_2$it is sufficient to calculate that of ε_1 via the Kramers–Kronig relations. This was achieved using the commercial software [13].

4. Results and discussion

The success of the model in fitting transmission data and its ability to extract parameter values comparable to those determined experimentally is now discussed. A further discussion is presented concerning the suitability of the model's initial assumptions.

Table 1 shows the experimental and modelled results for a selection of F doped ZnO films. The values of Δ_{BM}^{exp} and Δ_{BM}^{model} agree, typically within 5%, except for the samples with the lowest carrier concentrations where the error in determining such small shifts in the direct band gap becomes larger. For all samples, the modelled values of γ_w were ~0.5 eV. Values extracted for indirect band gaps were in the range 2.6 − 3.1 eV and, as for the effective direct band gaps, increased with doping concentration. However, it is not possible to put much confidence in the accuracy of these values due to the relatively small contribution to ε_2 compared with that for direct transitions.

Comparing the film thicknesses extracted using the Swanepoel method (d_S) and the model (d_{model}) it is clear that the values agree, although the model values are consistently higher by around 5%. The thickness values extracted by the model may be considered more accurate because it utilises all the experimental data points within the spectra and not just those located at maxima and minima of the fringes within the low-absorption region according to the Swanepoel method.

For each sample the model parameters were varied incrementally, according to the downhill simplex method, until the functional form of $\varepsilon(\omega)$ corresponding to minima in the MSE between experimental and theoretical transmission spectra was achieved. Fig. 2 shows an example of a typical fit to a transmission spectrum for a film deposited in a CHF_3 partial pressure of 5%. It is clear that the model achieves an excellent fit to the experimental spectra, there being a very low MSE of 0.6. The corresponding $n(\omega)$ and $\kappa(\omega)$ dispersion curves over the range 250 − 1000 nm are shown in Fig. 3. These curves fully characterise the material's optical response and can be used to re-create spectra of transmittance and reflectance for the film at any desired thickness using the transfer matrix method [23].

Fig. 4 shows the relative shapes of ε_2 for both undoped ZnO standard and ZnO:F sample, previously described by Figs. 2 and 3, in the region close to the direct band gap. For the undoped film, a value

Table 1
Experimental and modelled values obtained for a selection of F doped ZnO films.

CHF_3 (%)	d_S (nm)	n_e^H ($\times 10^{19}cm^{-3}$)	μ_e^H ($cm^2V^{-1}s^{-1}$)	E_g' (eV)	Δ_{BM}^{exp} (meV)	Δ_{BM}^{model} (meV)	γ_w (eV)	E_i (eV)	E_p (meV)	d_{model} (nm)	MSE (arb. units)
0	65	1.15	14.2	3.294	75	64	0.49	2.64	3.6	68	1.96
1	65	3.14	23.4	3.306	87	82	0.52	2.88	4.4	69	0.98
2	115	3.34	24.5	3.308	89	99	0.50	3.06	3.6	119	1.03
3	106	3.25	19.8	3.313	94	99	0.52	3.08	4.4	111	1.00
4	91	5.83	19.2	3.353	134	138	0.52	3.10	1.8	91	1.01
5	95	3.27	9.6	3.329	110	114	0.52	3.06	3.1	104	0.61

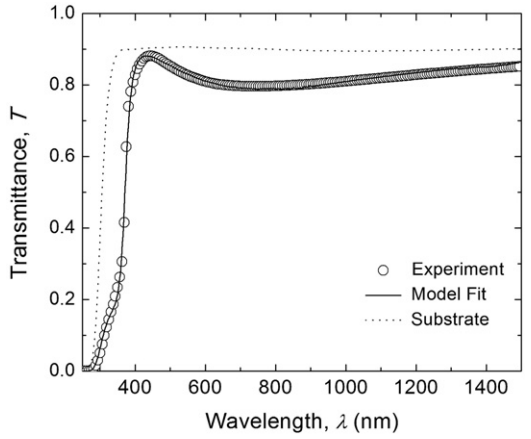

Fig. 2. Experimental transmission spectrum for a film with a carrier density of 3.27×10^{19} cm^{-3}. An excellent fit to the experimental data was achieved by the model with a MSE value of 0.6. Extracted values were $\Delta_{BM}^{model}=110$ meV, $\gamma_w=0.52$ eV, $E_i=3.06$ eV, $E_p=3.1$ meV and $d_{model}=104$ nm.

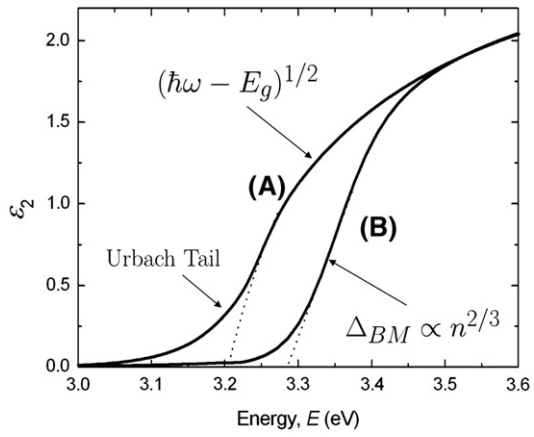

Fig. 4. The shape of the imaginary part of the dielectric function ε_2 extracted from the model for an undoped ZnO film (A) and a ZnO:F film sputtered in a 3% partial pressure of CHF_3 (B). For the undoped film a value of $E_d=3.19$ eV was extracted by setting $\Delta_{BM}=0$ eV. For the doped film values of $\Delta_{BM}=96$ meV and $\gamma_w=14$ meV were extracted from the model.

of $E_d=3.19$ eV (assuming $\Delta_{BM}^{model}=0$) was determined by the model, agreeing exactly with the experimentally determined value. The shape of the two curves differs by a factor of $(1-F_e)$ in the vicinity of the band gap as predicted by the effect of the Burstein–Moss shift, and re-converge at higher energies as expected.

The reliability of the model and the validity of its assumption will now be discussed: Firstly, the model assumes that the increase in the Fermi level, and hence the effective direct band gap, with carrier density is attributed solely to a BM shift (Eq. 13). However, it is apparent that a linear plot of Δ_{BM}^{exp} versus n_e^H (Fig. 5) does not extrapolate through the origin which suggests that there is a component to the increase in E_d that is not due to the BM shift alone. Thus, Eq. (13) must be re-written as

$$E_f = \frac{\hbar^2}{2m_e}(3\pi n_e)^{2/3} = \Delta_{BM} + \Delta_x \tag{18}$$

where Δ_x is the component to the shift not attributed to a BM effect. It may be speculated that this component is a consequence of the polycrystalline nature of the material and that its magnitude will be dependant on the overall grain structure of each of the doped films. Provided that Δ_x is independent of n_e it is still possible to make an estimate for the value of the effective electron mass m_e from the slope of the line in Fig. 5. A value of $m_e=0.33\pm0.08\ m_0$ was calculated. This value is higher than the value of $m_e=0.24\ m_0$ measured for undoped bulk ZnO [24]. This is expected as m_e has been shown to increase as a function of n_e[25] and the value is in accordance with other reported values for doped, polycrystalline ZnO [11,26]. Note that shifts in the band gap due to the presence of other phases, such as ZnF_2, are unlikely due to the high volatility of fluorides [27]. Indeed it has been shown that F doped ZnO films deposited by magnetron sputtering generally consist of a single ZnO phase [5].

Secondly, within the experimental range of investigation the use of a Drude component within the model for ZnO was redundant as the carrier concentrations in the films were not high enough to create a discernible change in the dielectric background. Thus, unless the experimental range of measurement or the carrier concentrations in future films is increased it is not necessary to include a Drude component. However, when the same modelling approach was applied to ITO films (not reported here) the Drude term was found to be essential in modelling the long wavelength behaviour of the optical transmission.

Currently, the maximum achievable n_e for reactively sputtered ZnO:F films is $\sim1\times10^{20}$ cm^{-3}[4]. Increasing n_e by a factor of 5 should result in ZnO:F films with resistivities low enough for them to be used as front contact layers in high performance CdTe/CdS solar cell devices. Alternative doping routes may be required to achieve this increase. For example, instead of using the reactive gas CHF_3, co-

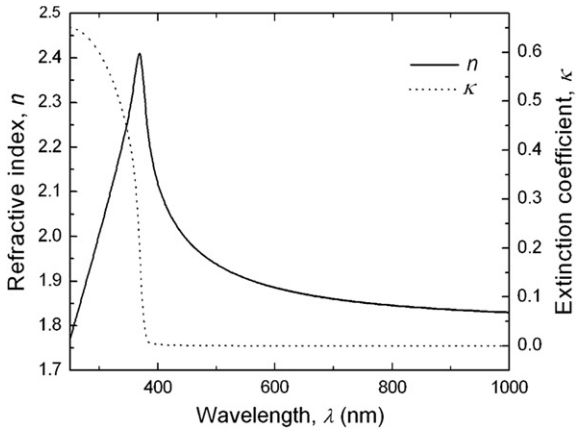

Fig. 3. Continuous curves of n and κ extracted from the model. Such curves fully describe the material's optical properties and can be used to generate transmittance and reflectance spectra via a simple transfer matrix method.

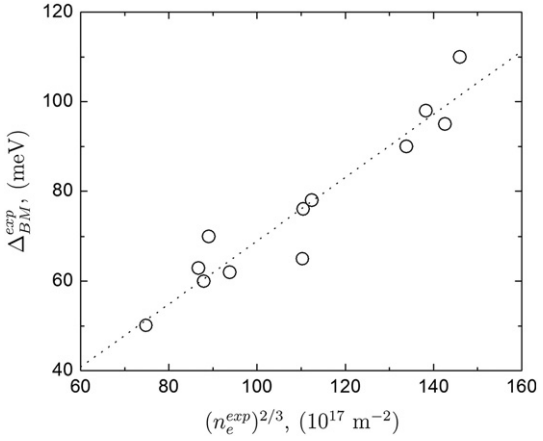

Fig. 5. Experimental values of the Burstein-shifts and carrier concentrations, determined via $(\alpha\hbar\omega)^2$ vs $\hbar\omega$ plots and van der Pauw measurements respectively, permit the estimation of the effective electron mass as $m_e=0.33\pm0.08$ m_0.

sputtering from separate targets of ZnO and ZnF_2 may prove a more efficient way of doping the films. The use of two separate targets will allow a combinatorial approach to determine the optimum sputtering parameters by incorporating a doping gradient across the resultant films. The application of the model presented in this work will permit the rapid profiling of opto-electronic properties across such combinatorial samples.

5. Conclusions

A successful model has been developed for the complex dielectric function $\varepsilon(\omega)$ for F doped ZnO that describes the effect of inter-band transitions (direct and indirect) according to a parabolic band assumption. Transmission data for multiple samples has been fitted with typical MSE values of <2. As a result, the model may be used to accurately extract $n(\omega)$ and $\kappa(\omega)$ for doped ZnO films which can then be incorporated with confidence into models of multi-layer structures such as CdTe/CdS solar cells. A value of $m_e = 0.33 \pm 0.08\, m_0$ was calculated from experimental data and is consistent with the previously published values. The Drude component within the model failed to improve the fit to transmission data due to its inapplicability to the range of wavelengths and doping densities studied. As a result further values for n_e and μ_e could not be extracted from the model. Nonetheless, it is hoped that the model will provide a useful characterisation tool for the rapid optimisation of fluorine doped ZnO films as further doping routes are explored.

Acknowledgements

The authors would like to thank Neil McSporran and Paul Warren of Pilkington for useful discussions and the provision of glass substrates. Funding for this work came from the EPSRC SUPERGEN PV-21 programme.

References

[1] S. Fay, J. Steinhauser, N. Oliveira, E. Vallat-Sauvain, C. Ballif, Thin Solid Films 515 (2007) 8558.
[2] T. Minami, T. Miyata, Y. Ohtani, Y. Mochizuki, Jpn. J. Appl. Phys. 45 (2006) 409.
[3] C. Agashe, O. Kluth, J. Hupkes, U. Zastrow, B. Rech, M. Wuttig, J. Appl. Phys. 95 (2004) 1911.
[4] R.E. Treharne, K. Durose, Thin Solid Films (2010), doi:10.1016/j.tsf.2010.12.126.
[5] Y. Tsai, N. Wang, C. Tsai, Mater. Lett. (2009) 1621.
[6] D. Ku, Y. Kim, K. Lee, T. Lee, B. Cheong, T. Seong, W. Kim, J. Electroceram. 23 (2009) 415.
[7] R. Swanepoel, J. Phys. E Sci. Instrum. 16 (1983) 1214.
[8] R. Swanepoel, J. Phys. E Sci. Instrum. 17 (1984) 896.
[9] Z. Li, D. Zhang, J. Lin, J. Appl. Phys. 99 (2006) 124906.
[10] Z. Qiao, C. Agashe, D. Mergel, Thin Solid Films 496 (2006) 520.
[11] A. Sarkar, S. Ghosh, S. Chaudhuri, A. Pal, Thin Solid Films 204 (1991) 255.
[12] D. Mergel, Z. Qiao, J. Phys. D Appl. Phys. 35 (2002) 794.
[13] M. Theiss, Scout 3.0, Hard and Software for Optical Spectroscopy, Dr. Bernhard-Klein-Str. 110, 52078 Aachen, Germany, www.mtheiss.com.
[14] F. Wooten, Optical Properties of Solids, Academic Press, New York, 1972.
[15] M. Dressel, G. Gruener, Electrodynamics of Solids: Optical Properties of Electrons in Matter, Cambridge University Press, Cambridge, 2002.
[16] P.P. Edwards, A. Porch, M.O. Jones, D.V. Morgan, R.M. Perks, Dalton Trans. (2004) 2995.
[17] I. Hamberg, C. Granqvist, J. Appl. Phys. 60 (1986) R123.
[18] T. Moss, G. Burrell, B. Ellis, Semiconductor opto-electronics, Butterworth, London, 1973.
[19] E. Burstein, Phys. Rev. 93 (1954) 632.
[20] T.S. Moss, Proc. Phys. Soc. B 67 (1954).
[21] S. O'Leary, S. Johnson, P. Lim, J. Appl. Phys. 82 (1997) 3334.
[22] R.A. Smith, Wave Mechanics of Crystalline Solids, Chapman and Hall, 1961.
[23] H.A. Macleod, Thin-Film Optical Filters, Adam Hilger Ltd, Bristol, 1986.
[24] W.S. Baer, Phys. Rev. 154 (1967) 785.
[25] F. Ruske, A. Pflug, V. Sittinger, B. Szyszka, D. Greiner, B. Rech, Thin Solid Films 518 (2009) 1289.
[26] S. Brehme, F. Fenske, W. Fuhs, E. Nebauer, M. Poschenrieder, B. Selle, I. Sieber, Thin Solid Films 342 (1999) 167.
[27] F. Yakuphanoglu, Y. Caglar, S. Ilican, M. Caglar, Phys. B Condens. Matter 394 (2007) 86.